

NORMAL MODES OF VORTICES IN EASY-PLANE FERROMAGNETS

G. M. Wysin

Department of Physics, Kansas State University, Manhattan, KS 66506 U.S.A.

A. R. Völkel

University of Toronto, Toronto, Ontario, Canada, M5S 1A7

(May 4, 1995)

We investigate the linear spin wave spectrum of 2d easy-plane classical Heisenberg ferromagnets in the presence of a vortex, using numerical diagonalization on small systems. The spectra of normal modes for both in-plane and out-of-plane vortices are determined, for square, triangular and hexagonal lattices. Some of the modes show a strong localization of their amplitudes near the center of the vortex. Moreover, we investigate a particular mode that drives the crossover in the static vortex structure from purely in-plane to a vortex with well-localized out-of-plane component as the easy-plane character of the system is reduced below a certain threshold.

PACS numbers: 75.10.Hk, 75.30.Ds, 75.40.Gb, 75.40.Mg

I. INTRODUCTION: VORTEX INSTABILITY

In classical models for quasi-two-dimensional magnetic materials¹, it has been found that vortex nonlinear excitations play an active role in phase transitions,^{2,3} and are expected to be important in the spin dynamics.⁴⁻⁶ The vortices are topologically stable excitations, carry effective charges, are created in particle-antiparticle pairs, and are expected to make contributions to correlation functions, especially, to central peak intensity in the dynamic structure function⁵ $S(\mathbf{q}, \omega)$. In particular, in models of three-component classical spins with easy-plane (XY) anisotropy, there are two types of vortices possible,^{7,8} known as “in-plane” and “out-of-plane” vortices, depending on whether the static vortex has zero or nonzero out-of-easy-plane spin components, respectively. For ferro- and antiferro-magnets, the static structure of the in-plane vortex is known exactly, while the static structure of the out-of-plane vortex is only known approximately (or numerically). Approximate results are also known for the modification of these spin structures for slowly moving vortices.^{8,9} Furthermore, the dynamics of pairs of vortices has received some study; for pairs of out-of-plane vortices, there are interesting orbital and translational relative motions with faster cyclotron-like oscillations superimposed.⁹⁻¹¹

Some attempts have been made to describe these motions as found from numerical simulations by effective equations of motion for the vortex centers,^{4,12,13} including effective masses and charges^{11,14,15} that determine the dynamics (collective coordinates.¹⁶) However, these approaches have assumed that a vortex has no internal dynamics, that a moving vortex consists of a uniformly translating spin profile of fixed shape, with no internal oscillations or other intrinsic time dependence. However, it is expected that the vortex spin profile can have some kind of internal oscillation, perhaps even when it is stationary (i.e., not translating), in analogy with the internal modes of nonlinear excitations in one dimension.¹⁷ Little is known about such dynamic modes of individual vortices. A description of their properties could be valuable in application to the collective coordinate theory¹⁸ and in calculations of dynamic response functions. These modes can be determined, however, by evaluating through numerical diagonalization the small amplitude normal modes of oscillation of the spin field about a single vortex. The resulting spinwave spectrum may contain particular modes that are strongly associated with the presence of the vortex itself, and otherwise absent if the vortex is absent. It is likely that these modes would be localized on the vortex. In addition, the spectrum will contain other modes that are extended over the entire system, and possibly only modified slightly by the presence of the vortex. Those modes, however, will contain information about the interaction of the spinwaves with the vortex. For these reasons, we investigate numerically the spinwave modes of a system containing an individual vortex, and analyze one particular spinwave mode that is responsible for an intrinsic instability^{8,19} of the in-plane vortex towards developing large out-of-plane spin components and becoming an out-of-plane vortex as the easy-plane anisotropy is reduced.

Specifically, we consider a set of classical spin variables on a two-dimensional (2D) lattice, interacting with easy-plane anisotropic near neighbor exchange. The easy-plane anisotropy will be described by the parameter λ ($0 \leq \lambda < 1$) in the following Hamiltonian:

$$H = -J \sum_{(\mathbf{n}, \mathbf{a})} (S_{\mathbf{n}}^x S_{\mathbf{n}+\mathbf{a}}^x + S_{\mathbf{n}}^y S_{\mathbf{n}+\mathbf{a}}^y + \lambda S_{\mathbf{n}}^z S_{\mathbf{n}+\mathbf{a}}^z). \quad (1.1)$$

The sum is over nearest neighbor pairs of spins S on a 2D lattice with sites $\{\mathbf{n}\}$, and the set of displacements to the nearest neighbors is $\{\mathbf{a}\}$.

Much of the theory for magnetic vortices in this model has been developed in continuum limits. In the present context, Costa *et al.*²⁰ and Pereira *et al.*²¹ have considered the spinwave modes about single vortices and vortex-antivortex pairs²² in the XY model ($\lambda = 0$), using a continuum limit description of the lattice. However, a continuum description of a magnetic vortex on a lattice presents difficulties, because the spin field varies rapidly from one lattice site to the next in the core region of the vortex, violating the usual continuum assumptions. Also, the short distance cutoff (for example, in energy integrals) in the continuum theory is not well-prescribed, whereas these difficulties do not appear if one solves for the spinwave modes in the original lattice model. For these reasons, we consider vortices in this model on a lattice, where the discrete lattice effects, that are most influential in the core of the vortex, can be correctly accounted for.

It is well-established that for this model with a specified strength of easy-plane anisotropy, only one of the vortex types is numerically stable when placed on a lattice.^{8,19} Numerical simulations have led to the conclusion that static in-plane vortices are stable only when λ is less than a critical value λ_c . On the other hand, static out-of-plane vortices are stable only when λ is greater than λ_c . To say that one type is unstable means that it will evolve into the other type. The critical value λ_c was found to have a substantial lattice-dependence; λ_c is approximately 0.62, 0.70, 0.84, for triangular, square, and hexagonal lattices, respectively (for ferromagnets). This strong lattice dependence is due partly to the discreteness effects near the vortex core, for which the usual continuum limit theories are likely to be inadequate.

This instability or crossover has been found to be driven by a particular dynamic mode of the in-plane vortex,²³ whose frequency goes to zero as λ approaches λ_c . Preliminary numerical diagonalizations were made for the spinwave modes of a 10×10 square lattice system containing one vortex, with a free boundary condition.^{9,24} A mode that became soft was found to have its amplitude concentrated near the center of the vortex, suggesting that it is a localized mode associated with the presence of the vortex, as opposed to an extended continuum spinwave mode of the entire system. More recently, an Ansatz was made for the structure of a vortex on a lattice,²³ in order to explain the lattice dependence of λ_c . In this Ansatz, it was assumed that only a small set of spins near the core of the vortex could have nonzero out-of-plane spin components, while all other spins farther out from the core were held fixed in the easy plane. The out-of-plane spin components were assumed to depend only on the radial distance from the vortex center. The analysis was used to determine very accurately the values of λ_c for the different lattices mentioned above. More importantly, it also was used to make estimates of the frequency of the dynamic mode responsible for the in-plane to out-of-plane vortex crossover. However, it is clear that a more complete analysis of the spinwave modes about a static vortex is needed, especially including an understanding of how that eigenfrequency depends on the system size.

Therefore, we have made a set of numerical diagonalizations for finite systems, to obtain the normal modes (i.e., spinwaves) in the presence of a single in-plane vortex for $\lambda < \lambda_c$, and in the presence of a single out-of-plane vortex for $\lambda > \lambda_c$. The calculations described here are semiclassical; the spin equations of motion have been linearized about a numerically-determined static vortex solution, using local Cartesian spin components with different local spin axes at each site. The notation for the calculation is described in the following section. Approximately circular systems on triangular, square, and hexagonal lattices were used. A set of calculations was performed for each lattice, with a range of system sizes. For each system used, the dependence of the eigenspectrum on the anisotropy λ was determined. This includes measuring the rms “sizes” of the wavefunctions associated with the modes, and comparing to the size of the finite system that was used, to decide which modes are localized and which are extended. The mode whose frequency approaches zero as λ approaches λ_c has occupied much of our attention. We give substantial analysis of its dependence on λ , the type of lattice, and the system size.

II. PERTURBATION ABOUT A STATIC VORTEX

We begin by describing how the numerical diagonalization problem for the normal modes of spinwave motion about a static vortex was set up. For classical states we can parameterize the spins in terms of an in-plane angle $\phi_{\mathbf{n}}$ and an out-of-plane angle $\theta_{\mathbf{n}}$, (or spin component), where $\sin \theta_{\mathbf{n}} \equiv S_{\mathbf{n}}^z/S$, i.e.,

$$\mathbf{S}_{\mathbf{n}} = S(\cos \theta_{\mathbf{n}} \cos \phi_{\mathbf{n}}, \cos \theta_{\mathbf{n}} \sin \phi_{\mathbf{n}}, \sin \theta_{\mathbf{n}}) \quad (2.1)$$

For in-plane vortices, the low energy static states of this model will have all $S_{\mathbf{n}}^z = \theta_{\mathbf{n}} = 0$, and then the equation to determine the in-plane angles becomes

$$H_{\text{red}} = -JS^2 \sum_{(\mathbf{n}, \mathbf{a})} \cos(\phi_{\mathbf{n}} - \phi_{\mathbf{n}+\mathbf{a}}) \quad (2.2)$$

$$\sum_{\mathbf{a}} \sin(\phi_{\mathbf{n}} - \phi_{\mathbf{n}+\mathbf{a}}) = 0. \quad (2.3)$$

Only when the vortex center (x_0, y_0) is at a point of high symmetry, such as the center of a unit cell of the lattice, or directly on a lattice site (with the spin at that lattice site set perpendicular to the easy-plane) is a simple analytic solution of Eq. (2.3) known, namely

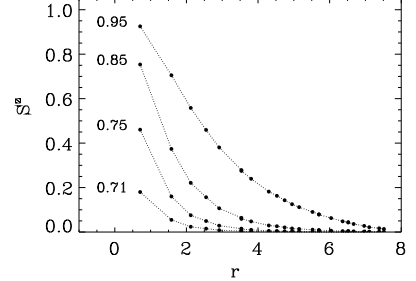
$$\phi_{\mathbf{n}} = q \arctan\left(\frac{y_{\mathbf{n}} - y_0}{x_{\mathbf{n}} - x_0}\right), \quad (2.4)$$

where the vorticity q is an integer. For out-of-plane vortices, the in-plane angles are given by Eq. (2.4), while there are nonzero $S_{\mathbf{n}}^z$ components. In general, for a given value of anisotropy λ , we have used a numerical relaxation procedure to determine the static vortex structure, for either in-plane or out-of-plane vortices. We start with an in-plane vortex, but perturb the spins in the unit cell containing the vortex core by giving only those sites small positive S^z components. Then every spin in the lattice is re-directed to point along the direction of the effective field $\mathbf{F}_{\mathbf{n}}$ due to its neighbors, as determined from the Hamiltonian above:

$$\mathbf{F}_{\mathbf{n}} = J \sum_{\mathbf{a}} [S_{\mathbf{n}+\mathbf{a}}^x \mathbf{e}_x + S_{\mathbf{n}+\mathbf{a}}^y \mathbf{e}_y + \lambda S_{\mathbf{n}+\mathbf{a}}^z \mathbf{e}_z]. \quad (2.5)$$

The set $\{\mathbf{a}\}$ includes only the displacements to the neighbors of site \mathbf{n} . Sites on the boundary of the finite system will tend to have weaker effective fields because of their smaller number of nearest neighbors in this sum. Upon iteration, this procedure relaxes the spins quickly into a static energy minimum vortex (in-plane or out-of-plane vortex) that is stable for the given value of anisotropy λ . This is because the spin equations of motion can be written in the form, $\dot{\mathbf{S}}_{\mathbf{n}} = \mathbf{S}_{\mathbf{n}} \times \mathbf{F}_{\mathbf{n}}$; the time derivatives vanish when the spins are aligned with the effective fields of their neighbors. The relaxed vortex configuration, $\mathbf{S}_{\mathbf{n}}^0 = (S_{\mathbf{n}}^x{}^0, S_{\mathbf{n}}^y{}^0, S_{\mathbf{n}}^z{}^0)$ can then be used to obtain the in-plane and out-of-plane angles of the static vortex, $(\phi_{\mathbf{n}}^0, \theta_{\mathbf{n}}^0)$, using the definition in Eq. (2.1). Some typical profiles of $S_{\mathbf{n}}^z{}^0$ so obtained for various values of $\lambda > \lambda_c \approx 0.70$ for a circular system on a square lattice are shown in Fig. 1.

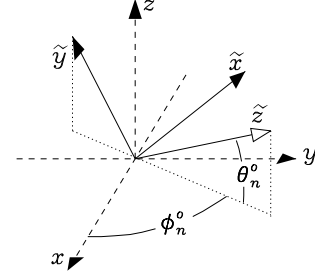
FIG. 1. Profiles of S^z vs. distance r from the vortex center, for single static out-of-plane vortices at the center of a circular system with 180 sites on a square lattice. The curves are labelled by the different values of λ . These results were obtained by the relaxation procedure described in the text (Sec. II), using a fixed boundary condition as described in Sec. IV.



Now the approach is to make the spinwave perturbation calculation using the directions, $\mathbf{S}_{\mathbf{n}}^0$, as the different local quantization axes for each site. This is similar in spirit to a spinwave calculation for an antiferromagnet,²⁵ in which the classical ground state can have sets of spins on the different sublattices aligned along different directions, and the perturbation analysis uses different coordinate systems for different sublattices. Usually, to determine the spinwave spectrum for some system, the small amplitude spin deviations are assumed to be relative to the local classical ground state directions. In the case here, the spin deviations are taken to be relative to a state with one vortex, which is not the ground state, but is a local energy minimum. Thus we rotate locally into new coordinates at each site, where the new axes for quantization of each site (\tilde{z} -axis) are along the spin directions for the relaxed vortex, while the new \tilde{x} -axis lies in the original xy -plane [See Fig. (2)]:

$$\begin{aligned} S_{\mathbf{n}}^x &= -S_{\mathbf{n}}^{\tilde{x}} \sin \phi_{\mathbf{n}}^0 - S_{\mathbf{n}}^{\tilde{y}} \sin \theta_{\mathbf{n}}^0 \cos \phi_{\mathbf{n}}^0 + S_{\mathbf{n}}^{\tilde{z}} \cos \theta_{\mathbf{n}}^0 \cos \phi_{\mathbf{n}}^0 \\ S_{\mathbf{n}}^y &= S_{\mathbf{n}}^{\tilde{x}} \cos \phi_{\mathbf{n}}^0 - S_{\mathbf{n}}^{\tilde{y}} \sin \theta_{\mathbf{n}}^0 \sin \phi_{\mathbf{n}}^0 + S_{\mathbf{n}}^{\tilde{z}} \cos \theta_{\mathbf{n}}^0 \sin \phi_{\mathbf{n}}^0 \\ S_{\mathbf{n}}^z &= S_{\mathbf{n}}^{\tilde{y}} \cos \theta_{\mathbf{n}}^0 + S_{\mathbf{n}}^{\tilde{z}} \sin \theta_{\mathbf{n}}^0 \end{aligned} \quad (2.6)$$

FIG. 2. Diagram showing the relation between the original xyz -coordinate system, and the local coordinates, $\tilde{x}\tilde{y}\tilde{z}$, where the \tilde{z} -axis lies along the direction of the spin at a particular site in the unperturbed vortex, and the \tilde{x} -axis lies in the xy -plane.



To simplify the notation that follows, we write

$$m_{\mathbf{n}}^0 = \sin \theta_{\mathbf{n}}^0, \quad p_{\mathbf{n}}^0 = \cos \theta_{\mathbf{n}}^0 \quad (2.7)$$

With this transformation, the Hamiltonian in the tilde coordinate system is

$$\begin{aligned} H = -J \sum_{\mathbf{n}} \sum_{\mathbf{m}=\mathbf{n}+\mathbf{a}} \{ & S_{\mathbf{n}}^{\tilde{x}} S_{\mathbf{m}}^{\tilde{x}} \cos(\phi_{\mathbf{n}}^0 - \phi_{\mathbf{m}}^0) \\ & + S_{\mathbf{n}}^{\tilde{y}} S_{\mathbf{m}}^{\tilde{y}} [m_{\mathbf{n}}^0 m_{\mathbf{m}}^0 \cos(\phi_{\mathbf{n}}^0 - \phi_{\mathbf{m}}^0) + \lambda p_{\mathbf{n}}^0 p_{\mathbf{m}}^0] \\ & + S_{\mathbf{n}}^{\tilde{z}} S_{\mathbf{m}}^{\tilde{z}} [p_{\mathbf{n}}^0 p_{\mathbf{m}}^0 \cos(\phi_{\mathbf{n}}^0 - \phi_{\mathbf{m}}^0) + \lambda m_{\mathbf{n}}^0 m_{\mathbf{m}}^0] \\ & + [S_{\mathbf{n}}^{\tilde{x}} S_{\mathbf{m}}^{\tilde{y}} m_{\mathbf{m}}^0 - S_{\mathbf{n}}^{\tilde{y}} S_{\mathbf{m}}^{\tilde{x}} m_{\mathbf{n}}^0 \\ & - S_{\mathbf{n}}^{\tilde{x}} S_{\mathbf{m}}^{\tilde{z}} p_{\mathbf{m}}^0 + S_{\mathbf{n}}^{\tilde{z}} S_{\mathbf{m}}^{\tilde{x}} p_{\mathbf{n}}^0] \sin(\phi_{\mathbf{n}}^0 - \phi_{\mathbf{m}}^0) \\ & + S_{\mathbf{n}}^{\tilde{y}} S_{\mathbf{m}}^{\tilde{z}} [-m_{\mathbf{n}}^0 p_{\mathbf{m}}^0 \cos(\phi_{\mathbf{n}}^0 - \phi_{\mathbf{m}}^0) + \lambda p_{\mathbf{n}}^0 m_{\mathbf{m}}^0] \\ & + S_{\mathbf{n}}^{\tilde{z}} S_{\mathbf{m}}^{\tilde{y}} [-p_{\mathbf{n}}^0 m_{\mathbf{m}}^0 \cos(\phi_{\mathbf{n}}^0 - \phi_{\mathbf{m}}^0) + \lambda m_{\mathbf{n}}^0 p_{\mathbf{m}}^0] \} \end{aligned} \quad (2.8)$$

The sums are over each bond in the lattice once. Sites on the edge of a finite system will contribute less, due to the smaller number of neighbors for those sites.

In what follows we impose semiclassical quantization by considering the operators $S_{\mathbf{n}}^{\tilde{x}}$, $S_{\mathbf{n}}^{\tilde{y}}$, $S_{\mathbf{n}}^{\tilde{z}}$ to be quantum operators, satisfying the Heisenberg equations of motion:

$$i\hbar \dot{\mathbf{S}}_{\mathbf{n}} = [\mathbf{S}_{\mathbf{n}}, H], \quad (2.9)$$

with the standard canonical commutators,

$$[S_{\mathbf{n}}^{\tilde{x}}, S_{\mathbf{m}}^{\tilde{y}}] = i\hbar S_{\mathbf{n}}^{\tilde{z}} \delta_{\mathbf{n},\mathbf{m}}, \quad (2.10)$$

and its cyclic permutations. Because we are studying the small amplitude deviations from the static vortex configuration, we need the equations of motion linearized in $S_{\mathbf{n}}^{\tilde{x}}$ and $S_{\mathbf{n}}^{\tilde{y}}$, with $S_{\mathbf{n}}^{\tilde{z}} \approx S$. Doing so, we obtain

$$\begin{aligned} \dot{S}_{\mathbf{n}}^{\tilde{x}} = JS \sum_{\mathbf{m}=\mathbf{n}+\mathbf{a}} \{ & m_{\mathbf{n}}^0 \sin(\phi_{\mathbf{n}}^0 - \phi_{\mathbf{m}}^0) S_{\mathbf{m}}^{\tilde{x}} \\ & + [p_{\mathbf{n}}^0 p_{\mathbf{m}}^0 \cos(\phi_{\mathbf{n}}^0 - \phi_{\mathbf{m}}^0) + \lambda m_{\mathbf{n}}^0 m_{\mathbf{m}}^0] S_{\mathbf{n}}^{\tilde{y}} \\ & - [m_{\mathbf{n}}^0 m_{\mathbf{m}}^0 \cos(\phi_{\mathbf{n}}^0 - \phi_{\mathbf{m}}^0) + \lambda p_{\mathbf{n}}^0 p_{\mathbf{m}}^0] S_{\mathbf{m}}^{\tilde{y}} \} \end{aligned} \quad (2.11a)$$

$$\begin{aligned} \dot{S}_{\mathbf{n}}^{\tilde{y}} = JS \sum_{\mathbf{m}=\mathbf{n}+\mathbf{a}} \{ & m_{\mathbf{m}}^0 \sin(\phi_{\mathbf{n}}^0 - \phi_{\mathbf{m}}^0) S_{\mathbf{m}}^{\tilde{y}} \\ & - [p_{\mathbf{n}}^0 p_{\mathbf{m}}^0 \cos(\phi_{\mathbf{n}}^0 - \phi_{\mathbf{m}}^0) + \lambda m_{\mathbf{n}}^0 m_{\mathbf{m}}^0] S_{\mathbf{n}}^{\tilde{x}} \\ & + \cos(\phi_{\mathbf{n}}^0 - \phi_{\mathbf{m}}^0) S_{\mathbf{m}}^{\tilde{x}} \} \end{aligned} \quad (2.11b)$$

Now we look for eigenstates or normal modes, in the sense that we try to find operators which are linear combinations of the $S_{\mathbf{n}}^{\tilde{x}}$ and $S_{\mathbf{n}}^{\tilde{y}}$ operators, with a single-frequency time dependence. Or, in quantum language, we look for creation and annihilation operators B_k^\dagger and B_k in which the Hamiltonian will be a sum of terms in the simple diagonal form $B_k^\dagger B_k$, where k is an index that distinguishes the different modes making up a complete set. While the equations are solved for finite systems, the usual momentum is not a good quantum number, due to the lack of translational

invariance. But the modes will be distinguished by the effective wavelengths of the standing waves present, and by the locations of nodes and antinodes in the wavefunctions or their squares. In any case, we suppose the modes are ordered in some way, perhaps from largest to smallest frequency, and notated by an index k . Some modes may be energetically degenerate, in which case k must denote more than just the frequency. It is clear that this type of problem will produce pairs of conjugate modes, B_k and B_k^\dagger , and we suppose these unknown operators are the linear combinations,

$$B_k^\dagger = \sum_{\mathbf{n}} (w_{k,\mathbf{n}}^1 S_{\mathbf{n}}^{\tilde{x}} + w_{k,\mathbf{n}}^2 S_{\mathbf{n}}^{\tilde{y}}) \quad (2.12a)$$

together with the conjugate definition,

$$B_k = \sum_{\mathbf{n}} (w_{k,\mathbf{n}}^{1*} S_{\mathbf{n}}^{\tilde{x}} + w_{k,\mathbf{n}}^{2*} S_{\mathbf{n}}^{\tilde{y}}) \quad (2.12b)$$

where the complex expansion coefficients $w_{k,\mathbf{n}}^1$ and $w_{k,\mathbf{n}}^2$ are to be determined. (This being a linear problem, there should be no confusion that the superscripts “1” and “2” are not powers.) With the requirement of $\exp i\omega_k t$ time dependence, where ω_k is the unknown eigenfrequency to be determined, B_k^\dagger must satisfy

$$\dot{B}_k^\dagger = i\omega_k B_k^\dagger. \quad (2.13)$$

Using Eqs. (2.12) and (2.11) in Eq. (2.13) leads to the following matrix equation for the coefficients:

$$\begin{aligned} i\omega_k w_{k,\mathbf{n}}^1 = JS \sum_{\mathbf{m}=\mathbf{n}+\mathbf{a}} \{ & -m_{\mathbf{m}}^0 \sin(\phi_{\mathbf{n}}^0 - \phi_{\mathbf{m}}^0) w_{k,\mathbf{m}}^1 \\ & + \cos(\phi_{\mathbf{n}}^0 - \phi_{\mathbf{m}}^0) w_{k,\mathbf{m}}^2 \\ & - [p_{\mathbf{n}}^0 p_{\mathbf{m}}^0 \cos(\phi_{\mathbf{n}}^0 - \phi_{\mathbf{m}}^0) + \lambda m_{\mathbf{n}}^0 m_{\mathbf{m}}^0] w_{k,\mathbf{n}}^2 \} \end{aligned} \quad (2.14a)$$

$$\begin{aligned} i\omega_k w_{k,\mathbf{n}}^2 = JS \sum_{\mathbf{m}=\mathbf{n}+\mathbf{a}} \{ & -m_{\mathbf{n}}^0 \sin(\phi_{\mathbf{n}}^0 - \phi_{\mathbf{m}}^0) w_{k,\mathbf{m}}^2 \\ & - [m_{\mathbf{n}}^0 m_{\mathbf{m}}^0 \cos(\phi_{\mathbf{n}}^0 - \phi_{\mathbf{m}}^0) + \lambda p_{\mathbf{n}}^0 p_{\mathbf{m}}^0] w_{k,\mathbf{m}}^1 \\ & + [p_{\mathbf{n}}^0 p_{\mathbf{m}}^0 \cos(\phi_{\mathbf{n}}^0 - \phi_{\mathbf{m}}^0) + \lambda m_{\mathbf{n}}^0 m_{\mathbf{m}}^0] w_{k,\mathbf{n}}^1 \} \end{aligned} \quad (2.14b)$$

For numerical diagonalization, the lattice sites are numbered in some arbitrary order, and then a vector can be formed out of the $w_{k,\mathbf{n}}^1$ and $w_{k,\mathbf{n}}^2$ variables as

$$(w_1^1, w_1^2, w_2^1, w_2^2, w_3^1, w_3^2, \dots) \quad (2.15)$$

This will allow Eqs. (2.14) to be solved numerically for the eigenvalues ω_k and their respective eigenvectors, given in terms of the coefficients $w_{\mathbf{n}}^1$ and $w_{\mathbf{n}}^2$. In this notation, the matrix to be diagonalized is real, but not Hermitian.

Once we have the complete set of these normal modes and their eigenfrequencies, the Hamiltonian will be expressed in the diagonal form;

$$H_{sw} = \sum_k \hbar \omega_k B_k^\dagger B_k, \quad (2.16)$$

where B_k and B_k^\dagger have equal frequencies, but with opposite signs.

III. NORMALIZATION, SPIN EXPECTATIONS AND FLUCTUATIONS

The complete eigenspectrum will contain all the information needed to determine the expectation values and fluctuations of the individual spins in the system, either for a single spinwave mode, or, for the system in thermal equilibrium. To determine expectation values of the spin components or their squares, we need to know $S_{\mathbf{n}}^{\tilde{x}}$ and $S_{\mathbf{n}}^{\tilde{y}}$ in terms of the normal modes B_k and B_k^\dagger . This means we need to invert the defining relations (2.12). First of all, the overall normalization of B_k and B_k^\dagger must be chosen so that their commutator is unity, $[B_k, B_{k'}^\dagger] = \delta_{k,k'}$. From the definitions, we must require

$$[B_k, B_k^\dagger] = \hbar S \sum_{\mathbf{n}} [(i w_{k,\mathbf{n}}^1 w_{k,\mathbf{n}}^2)^* + (i w_{k,\mathbf{n}}^1 w_{k,\mathbf{n}}^2)^*] = 1. \quad (3.1)$$

where $S_{\mathbf{n}}^{\tilde{z}} \rightarrow S$ was used. We assume in what follows that the $w_{k,\mathbf{n}}^1$ and $w_{k,\mathbf{n}}^2$ coefficients are now rescaled to give the unit normalization and unit commutator of B_k with B_k^\dagger in Eq. (3.1). Then, the following inverse expressions are assumed,

$$S_{\mathbf{n}}^{\tilde{x}} = \sum_k (e_{\mathbf{n},k}^1 B_k + e_{\mathbf{n},k}^2 B_k^\dagger) \quad (3.2a)$$

$$S_{\mathbf{n}}^{\tilde{y}} = \sum_k (e_{\mathbf{n},k}^3 B_k + e_{\mathbf{n},k}^4 B_k^\dagger). \quad (3.2b)$$

To determine the new coefficients $e_{\mathbf{n},k}^1$ and $e_{\mathbf{n},k}^2$ in terms of the $w_{k,\mathbf{n}}^1$ and $w_{k,\mathbf{n}}^2$ coefficients, one can form the commutator of B_k or B_k^\dagger [Eqs. (2.12)] with $S_{\mathbf{n}}^{\tilde{x}}$ and with $S_{\mathbf{n}}^{\tilde{y}}$, giving

$$[B_k^\dagger, S_{\mathbf{n}}^{\tilde{x}}] = -i\hbar w_{k,\mathbf{n}}^2 S_{\mathbf{n}}^{\tilde{z}} \approx -i\hbar S w_{k,\mathbf{n}}^2, \quad (3.3a)$$

$$[B_k, S_{\mathbf{n}}^{\tilde{x}}] = -i\hbar w_{k,\mathbf{n}}^{2*} S_{\mathbf{n}}^{\tilde{z}} \approx -i\hbar S w_{k,\mathbf{n}}^{2*}, \quad (3.3b)$$

$$[B_k^\dagger, S_{\mathbf{n}}^{\tilde{y}}] = i\hbar w_{k,\mathbf{n}}^1 S_{\mathbf{n}}^{\tilde{z}} \approx i\hbar S w_{k,\mathbf{n}}^1, \quad (3.3c)$$

$$[B_k, S_{\mathbf{n}}^{\tilde{y}}] = i\hbar w_{k,\mathbf{n}}^{1*} S_{\mathbf{n}}^{\tilde{z}} \approx i\hbar S w_{k,\mathbf{n}}^{1*}. \quad (3.3d)$$

On the other hand, forming the commutator of B_k and B_k^\dagger with $S_{\mathbf{n}}^{\tilde{x}}$ and $S_{\mathbf{n}}^{\tilde{y}}$ [Eq. (3.2)] leads to equivalent results,

$$[B_k^\dagger, S_{\mathbf{n}}^{\tilde{x}}] = -e_{\mathbf{n},k}^1, \quad [B_k, S_{\mathbf{n}}^{\tilde{x}}] = e_{\mathbf{n},k}^2, \quad (3.4a)$$

$$[B_k^\dagger, S_{\mathbf{n}}^{\tilde{y}}] = -e_{\mathbf{n},k}^3, \quad [B_k, S_{\mathbf{n}}^{\tilde{y}}] = e_{\mathbf{n},k}^4. \quad (3.4b)$$

Thus there is the conversion between the coefficients;

$$e_{\mathbf{n},k}^1 = i\hbar S w_{k,\mathbf{n}}^2, \quad e_{\mathbf{n},k}^2 = e_{\mathbf{n},k}^{1*} \quad (3.5a)$$

$$e_{\mathbf{n},k}^3 = -i\hbar S w_{k,\mathbf{n}}^1, \quad e_{\mathbf{n},k}^4 = e_{\mathbf{n},k}^{3*} \quad (3.5b)$$

As an application of these results, we can determine the local magnetization for a site by finding an expectation value of the original lab frame spin components, to quadratic order in the creation and annihilation operators. In order to do this, we first need expectation values of the spin components in the tilde coordinate system. From their definitions, $\langle S_{\mathbf{n}}^{\tilde{x}} \rangle = \langle S_{\mathbf{n}}^{\tilde{y}} \rangle = 0$, because these are linear in B_k and B_k^\dagger . However, the \tilde{z} component will be reduced slightly below S due to spin fluctuations of the modes. In order to preserve the overall spin length and the commutation relations of $S_{\mathbf{n}}^{\tilde{x}}$ and $S_{\mathbf{n}}^{\tilde{y}}$ with $S_{\mathbf{n}}^{\tilde{z}}$, it is necessary to use the following expression for $S_{\mathbf{n}}^{\tilde{z}}$ (as in the standard Holstein-Primakoff²⁶ transformation):

$$S_{\mathbf{n}}^{\tilde{z}} = S - \frac{1}{2S} (S_{\mathbf{n}}^{\tilde{x}} - iS_{\mathbf{n}}^{\tilde{y}})(S_{\mathbf{n}}^{\tilde{x}} + iS_{\mathbf{n}}^{\tilde{y}}), \quad (3.6)$$

where the latter terms are the spin lowering and raising operators. Using Eq. (3.2) and Eq. (3.5), the expectation value of this expression is

$$\begin{aligned} \langle S_{\mathbf{n}}^{\tilde{z}} \rangle &= S - \frac{S}{2} \sum_k \{ |w_{k,\mathbf{n}}^1 + i w_{k,\mathbf{n}}^2|^2 \langle B_k^\dagger B_k \rangle \\ &\quad + |w_{k,\mathbf{n}}^1 - i w_{k,\mathbf{n}}^2|^2 \langle B_k B_k^\dagger \rangle \}, \end{aligned} \quad (3.7)$$

where terms linear in the B_k and B_k^\dagger operators and terms like $\langle B_k B_q \rangle$ and $\langle B_k^\dagger B_q^\dagger \rangle$ are zero in the unperturbed (single-vortex) state and in single-quantum states and therefore do not appear here. The expectation values of the B_k and B_k^\dagger operators will be determined by the type of state, whether it be a state with one mode excited or a thermodynamic ensemble of states (equilibrium state). For example, if the state that we are perturbing from (single vortex) is denoted $|0\rangle$, then single-quantum excited states are denoted, $|k\rangle$,

$$|k\rangle = B_k^\dagger |0\rangle. \quad (3.8)$$

The fundamental expectation values are $\langle 0|B_k^\dagger B_k|0\rangle = 0$, and $\langle 0|B_k B_k^\dagger|0\rangle = 1$. On the other hand, if the interest is in a thermal ensemble, then the expectation value required will be the Bose-Einstein occupation, $\langle B_k^\dagger B_k \rangle = [\exp(\beta\hbar\omega_k) - 1]^{-1}$, where $\beta = k_B T$ is the inverse temperature. It is clear that the expectation values of the $S^{\tilde{z}}$ components will be less than S as a result of fluctuations, while the expectation values of $S^{\tilde{x}}$ and $S^{\tilde{y}}$ will be zero. As a result, it is straightforward to use Eq. (3.7) in the coordinate transformation Eq. (2.6) to obtain the expectation values in the original lab coordinates, i.e., the spin is just reduced in effective length,

$$\begin{aligned} \langle \mathbf{S}_n \rangle &= \langle S_n^{\tilde{z}} \rangle (\cos \theta_n^0 \cos \phi_n^0, \cos \theta_n^0 \sin \phi_n^0, \sin \theta_n^0) \\ &= \langle S_n^{\tilde{z}} \rangle \mathbf{S}_n^0 / S \end{aligned} \quad (3.9)$$

We also want to know the spin fluctuations associated with some state. The spin fluctuations will be defined in terms of squares of Cartesian spin components, relative to the vortex state. For instance, the in-plane and out-of-plane spin fluctuations are described by

$$\begin{aligned} \langle (\delta S_n^{\text{in}})^2 \rangle &= \langle (S_n^x - \langle S_n^x \rangle)^2 + (S_n^y - \langle S_n^y \rangle)^2 \rangle, \\ \langle (\delta S_n^{\text{out}})^2 \rangle &= \langle (S_n^z - \langle S_n^z \rangle)^2 \rangle. \end{aligned} \quad (3.10)$$

Using the definitions of the tilde coordinates, Eq. (2.6), these are equivalent to

$$\langle (\delta S_n^{\text{in}})^2 \rangle = \langle S_n^{\tilde{x}2} \rangle + \langle S_n^{\tilde{y}2} \rangle \sin^2 \theta_n^0 \quad (3.11a)$$

$$\langle (\delta S_n^{\text{out}})^2 \rangle = \langle S_n^{\tilde{z}2} \rangle \cos^2 \theta_n^0 \quad (3.11b)$$

Making use of the expansion of spin components in the operators B_k and B_k^\dagger , Eq. (3.2), together with Eq. (3.5), one can write the fluctuations in the tilde coordinates,

$$\langle S_n^{\tilde{x}2} \rangle = (\hbar S)^2 \sum_k |w_{k,n}^2|^2 \langle 2B_k^\dagger B_k + 1 \rangle, \quad (3.12a)$$

$$\langle S_n^{\tilde{y}2} \rangle = (\hbar S)^2 \sum_k |w_{k,n}^1|^2 \langle 2B_k^\dagger B_k + 1 \rangle. \quad (3.12b)$$

Finally, the resulting in-plane and out-of-plane fluctuations are:

$$\begin{aligned} \langle (\delta S_n^{\text{in}})^2 \rangle &= (\hbar S)^2 \sum_k \left(|w_{k,n}^2|^2 + |w_{k,n}^1|^2 \sin^2 \theta_n^0 \right) \\ &\quad \times \langle 2B_k^\dagger B_k + 1 \rangle \end{aligned} \quad (3.13a)$$

$$\begin{aligned} \langle (\delta S_n^{\text{out}})^2 \rangle &= (\hbar S)^2 \sum_k |w_{k,n}^1|^2 \cos^2 \theta_n^0 \\ &\quad \times \langle 2B_k^\dagger B_k + 1 \rangle \end{aligned} \quad (3.13b)$$

IV. NUMERICAL APPLICATION

First, for a given value of λ , the static vortex structure was found using the relaxation procedure described in Section II. This static structure acquires nonzero out-of-plane spin components for $\lambda > \lambda_c$. Then, the eigenvalue problem [Eq. (2.14)] was solved numerically for the eigenvectors and corresponding eigenvalues, for systems with hundreds of sites. Because there are two variables per site, the size of the matrix to diagonalize is $2N \times 2N$, where N is the number of sites in the lattice. Calculations were performed for approximately circular shaped systems, with the vortex centered in the system. For these finite systems, there is a choice of either a free boundary condition or a fixed boundary condition. For the free boundary condition, the lattice is cut off along a circular boundary, and then the sites on the edge of the system simply have a lower coordination number than those in the interior, and have a lower effective stiffness as a result. For the fixed boundary condition, the set of spins on the boundary of the system is coupled to an extra set of spins that are outside the system, still on the same lattice, but held fixed in the directions that the static in-plane vortex would give them. In this way, even the spins at the edge of the system have the same coordination number as those in the interior, however, they are coupled to spins that do not move that are outside the system. Therefore, this fixed boundary condition, which is stiffer than the free boundary condition, tends to give higher eigenfrequencies. Additionally, the fixed boundary condition results in values for λ_c that converge faster to a limit with increasing system size, and for this reason, most of the results reported here were produced with fixed boundary conditions.

For a given system, the eigenspectrum was determined for a sequence of closely spaced values of λ between 0 and 1. An eigenvector for one value of λ was projected onto the eigenvectors for the previous value of λ , and then identified with the one with which the overlap was the greatest. This allowed the eigenfrequencies for the different modes to be tracked as a function of λ . For a system with N sites, N modes of positive frequency, corresponding to the B_k^\dagger operators, resulted, along with an equivalent set of N modes of negative frequency, corresponding to the conjugate B_k operators. Double precision was used so that degenerate pairs of eigenmodes could be unambiguously identified, a necessity for performing the eigenvector overlaps.

V. RESULTS: SQUARE LATTICE

Calculations on systems with $4 \leq N \leq 492$ were made. For the fixed boundary condition used, the lowest frequency mode is the mode which becomes soft at some $\lambda_c < 1$. On the other hand, when free boundary conditions are used, there are also a few modes that can lie below the soft mode, reflecting the greater freedom of movement of the boundary spins; the lowest mode is at $\omega = 0$, corresponding to a uniform rotation of all the spins in the easy-plane, a motion that is frozen out by the fixed boundary condition. Some typical spectra (ω_k for B_k^\dagger) for the two different boundary conditions are shown in Fig. 3 for a 180 site system. For both types of boundary conditions in Fig. 3, out-of-plane spin components are present in the static vortex for $\lambda > 0.70 \approx \lambda_c$.

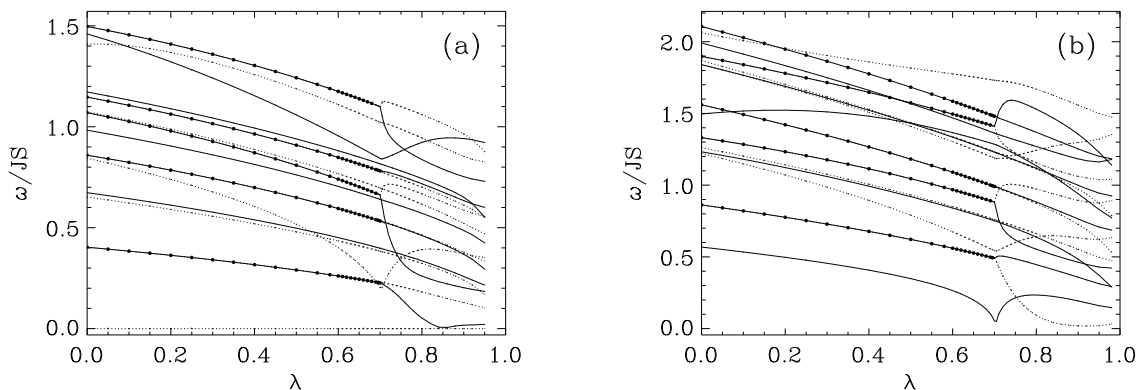


FIG. 3. Comparison of the lowest 19 modes in the spinwave spectrum for a square lattice circular system with 180 sites, containing an in-plane vortex at its center, with (a) free boundary conditions, and (b) fixed boundary conditions. Degenerate modes are marked with solid circles. The solid and dotted lines are used only to distinguish nearby modes.

There are some striking features of these results, which are typical of all the eigenspectrum results for different sized systems and lattices. Consider the fixed boundary condition (Fig. 3b). One mode of the in-plane vortex (the lowest mode) comes close to zero frequency as λ approaches λ_c from below. This mode is still present for $\lambda > \lambda_c$, with the out-of-plane vortex as static structure, and its frequency again rises away from zero. The spectrum suggests that this mode can be considered as a soft mode that is responsible for the energetic instability of an in-plane vortex to become an out-of-plane vortex, and vice-versa, as $|\lambda - \lambda_c| \rightarrow 0$. The other obvious feature of the spectrum is that modes that are degenerate (solid circles) for the in-plane vortex become split for the out-of-plane vortex. This change also occurs for λ near λ_c . It is likely that the degeneracy for $\lambda < \lambda_c$ for the in-plane vortex comes about because these modes have an S^z component that can be essentially “up” or “down”. On the other hand, for the out-of-plane vortex, this up-down symmetry is certainly violated, because the static spin configuration already possesses a nonzero S^z profile. Also, one of the modes that comes out of the lowest degenerate pair goes very close to zero frequency for λ near 0.9.

There are some differences for the free boundary condition, Fig. 3a. Here the “soft mode” that bears the most resemblance to that for the fixed boundary condition reaches a downward cusp at λ_c , but does not go below $\omega/JS \approx 0.15$. On the other hand, this is the value of λ above which the lowest degenerate mode becomes nondegenerate, one component of which *does* go very close to zero frequency near $\lambda = 0.84$, and then rises up again. For both boundary conditions, there are actually several modes higher up in the spectra that also come to downward cusps near λ_c , while other modes show no particular features near λ_c .

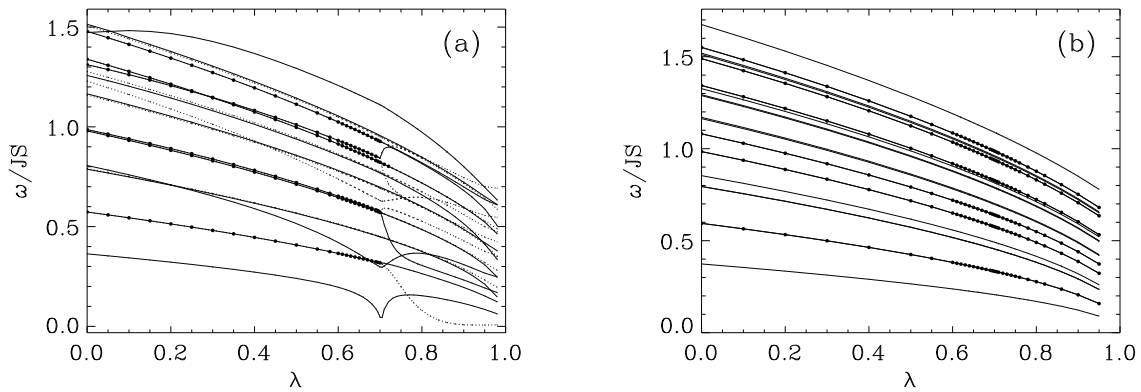
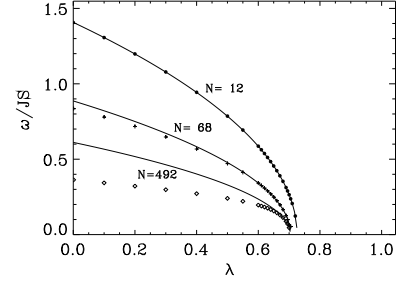


FIG. 4. Comparison of the lowest 19 modes in the spinwave spectrum for a square lattice circular system with 492 sites, with fixed boundary conditions, (a) containing an in-plane vortex at its center, and (b) no vortex (spinwave modes about ferromagnetically aligned state). The solid and dotted lines are used only to distinguish nearby modes.

We can also consider how the size of the system affects the low-frequency spectrum. For example, the lower part of the spectrum for a system with 492 sites is shown in Fig. 4a. In general the low-frequency modes found for the 180-site system are also seen in the 492-site system, but slightly shifted in frequency. The same sets of two-fold degeneracies are also found, which are again related to a symmetry in S^z for these modes of the in-plane vortex. And, once again, there are modes higher up in the spectrum with downward cusps at $\lambda = \lambda_c$.

In Fig. 4b, the low-frequency spectrum for the 492-site system *without* a vortex is shown. The sites were initially aligned in the xy -plane ferromagnetically. We find more or less the same sequence of nondegenerate and degenerate modes, which do not split at any λ . There is no mode that goes soft, as expected, since the ferromagnetic state is a stable energy minimum for $0 \leq \lambda < 1$, and there are no cusps.

FIG. 5. Asymptotic least square fits (solid curves) of the frequency of the soft mode (data points) for square lattice circular systems with 12, 68, and 492 spins, using the functional form $\omega = \hat{\omega}(1 - \lambda/\lambda_c)^{1/2}$. Only the data with λ very close to λ_c were used to obtain the fitted curves. This functional form fits well over the full range of λ only for small systems ($N \leq 24$).

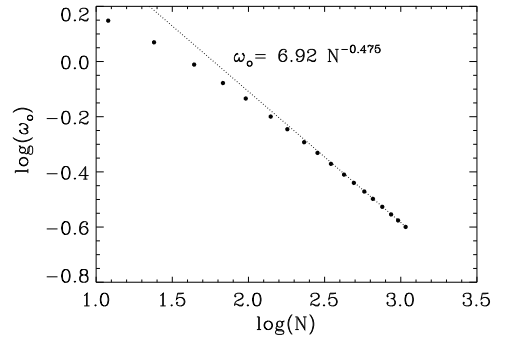


For fixed boundary conditions, the soft mode for $\lambda < \lambda_c$ has been fit to the following functional form, as suggested through the simple Ansatz by Wysin²³;

$$\omega = \hat{\omega} \sqrt{1 - \lambda/\lambda_c}, \quad (5.1)$$

where $\hat{\omega}$ and λ_c are the fitting parameters. Generally, if all the data where $\omega > 0$ are used in the fit, this functional form produces an accurate fit only for the smaller systems, up to about 24 spins. More generally, we can use only a limited number of the data points nearest to the zero frequency point, and apply this form there to estimate λ_c . Some typical asymptotic fits are shown in Fig. 5, for systems with 12, 68, and 492 spins. The values of λ_c determined this way converge to a limit near $\lambda_c \approx 0.70$ for the infinite sized system. The frequency of the soft mode at $\lambda = 0$, $\omega_o \equiv \omega(\lambda = 0)$, gives an indication of the overall frequency scale for this mode, and is shown in Fig. 6, versus system size (numbers not obtained from any fitting). The result is compared with an asymptotic fit to the function, $\omega_o = 6.92N^{-0.475}$. This is close to a linear dependence on inverse system length.

FIG. 6. Size dependence of the soft mode for square lattice circular systems with N sites, using fixed boundary conditions. The frequency ω_o of the soft mode at $\lambda = 0$ is shown on a log-log plot, and compared with an asymptotic fit to the function, $\omega_o = 6.92N^{-0.475}$. This is close to a linear dependence on inverse system diameter.



The above results show how there is one particular mode that goes soft for $\lambda \rightarrow \lambda_c$. To get a better idea of the physical structure of this mode or any of the modes, it is necessary to look at the associated wavefunctions. Also, it is important to measure the spread of the wavefunctions, to understand whether a particular mode is localized on the vortex or extended throughout the system. For a system with 180 spins, the wavefunctions of the six lowest energy modes are shown in Figs. 7, 8, 9, for $\lambda = 0$, $\lambda = 0.69$, and $\lambda = 0.76$, corresponding to well below λ_c , just below λ_c , and slightly above λ_c .

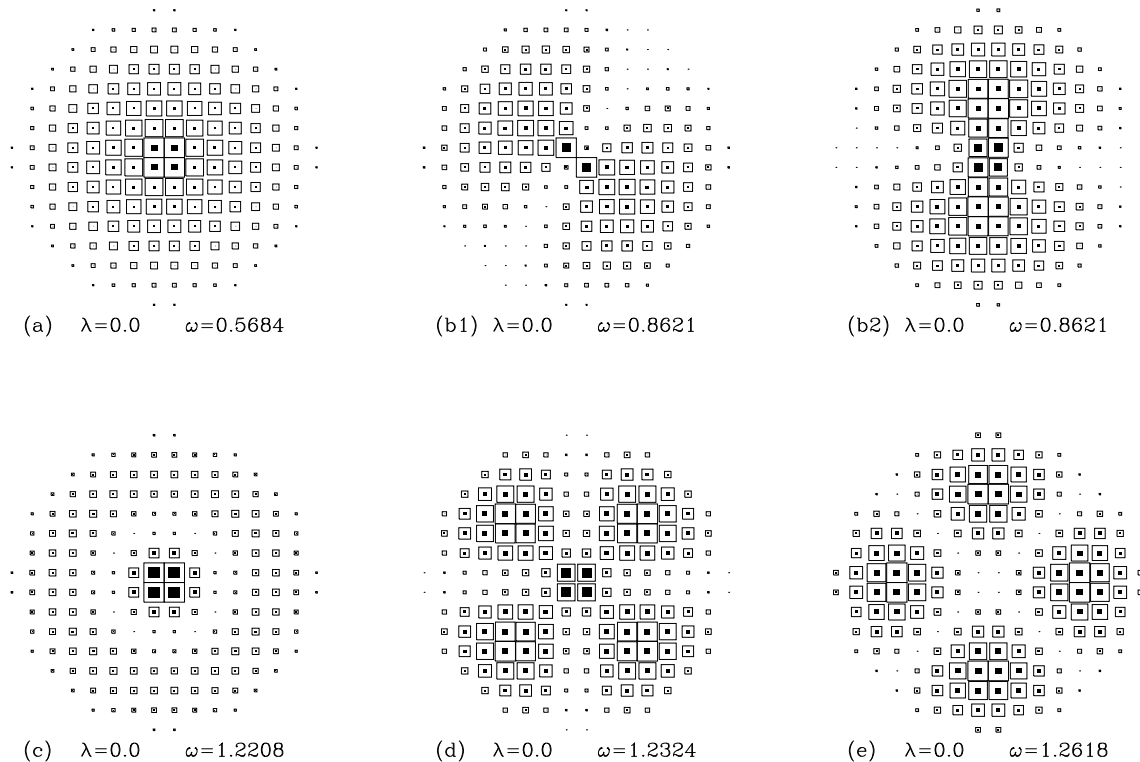


FIG. 7. Maps of the spin fluctuations in a square lattice system with 180 sites, for the six lowest frequency modes when $\lambda = 0.0$. Out-of-plane fluctuations $\langle (\delta S_{\mathbf{n}}^{\text{out}})^2 \rangle$ (Eq. 3.13b) are proportional to the areas of the solid squares. In-plane fluctuations $\langle (\delta S_{\mathbf{n}}^{\text{in}})^2 \rangle$ (Eq. 3.13a) are proportional to the white area within the larger squares. The total in-plane plus out-of-plane fluctuations are proportional to the areas of the larger squares. Part (a) shows the soft mode, while (b1) and (b2) are a degenerate pair, and (c), (d) and (e) are the next higher frequency modes.

In these diagrams, two squares representing the squared wavefunction are plotted at each lattice site, in order to present both the in-plane and out-of-plane fluctuations for the selected mode on one diagram. The area of the inner solid square is proportional to the out-of-plane spin fluctuations for that site, as in Eq. (3.13b). The area of the larger open square is proportional to the total in-plane plus out-of-plane spin fluctuations, as in Eq. (3.13). The difference of the two areas (the white area outside the solid square, and inside the open square) is proportional to the in-plane spin fluctuations, as in Eq. (3.13a). For the soft mode (a), there is a substantial increase in the out-of-plane fluctuations as λ approaches λ_c , while the relative size of the in-plane fluctuations diminishes. For the other lowest modes, there are only minor changes in the fluctuations with λ . The mode labeled (b) is doubly degenerate, while (b1) and (b2) are its two components that are split above λ_c [Fig. 9]. Also note that the orientation of the two components of this mode is rather arbitrary, because there is an arbitrary phase between the two modes involved. This is the cause for the oblique angle of the line of nodes in mode (b1) in Figures 7 and 10.

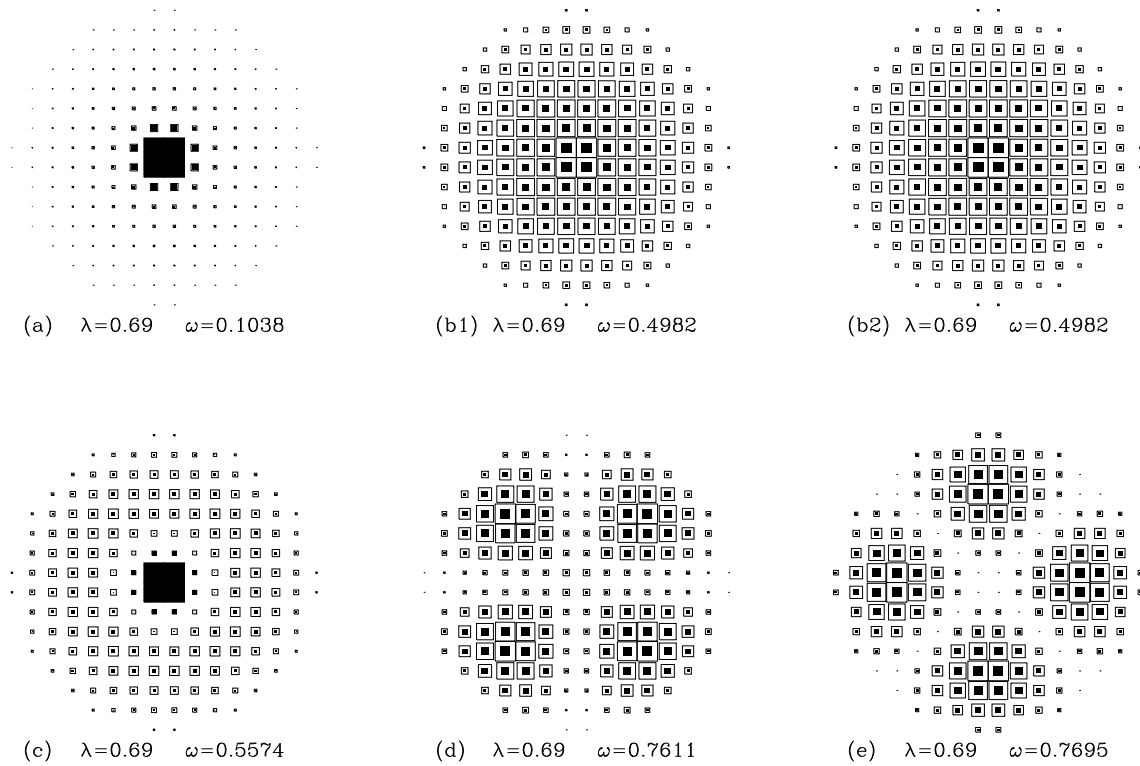


FIG. 8. Maps of the spin fluctuations in the square lattice system as in Fig. 7, but for $\lambda = 0.69$, just below the transition to an out-of-plane vortex. In (a), the soft mode's intensity concentrates itself more near the vortex core, and is strongly out-of-plane, while the higher modes in (b) through (e) have much smaller changes from their $\lambda = 0.0$ forms.

For comparison, Fig. 10 shows the lowest modes on the 180-site system in the absence of the vortex, at $\lambda = 0$, starting instead from a ferromagnetically aligned state. Some modes, including the one that most resembles the soft mode when the vortex is present, do not appear very different whether the vortex is present or absent (for this value of λ far from λ_c). On the other hand, some modes, such as (b) and (d), clearly have amplitude at the vortex core that is not present when the vortex is removed.

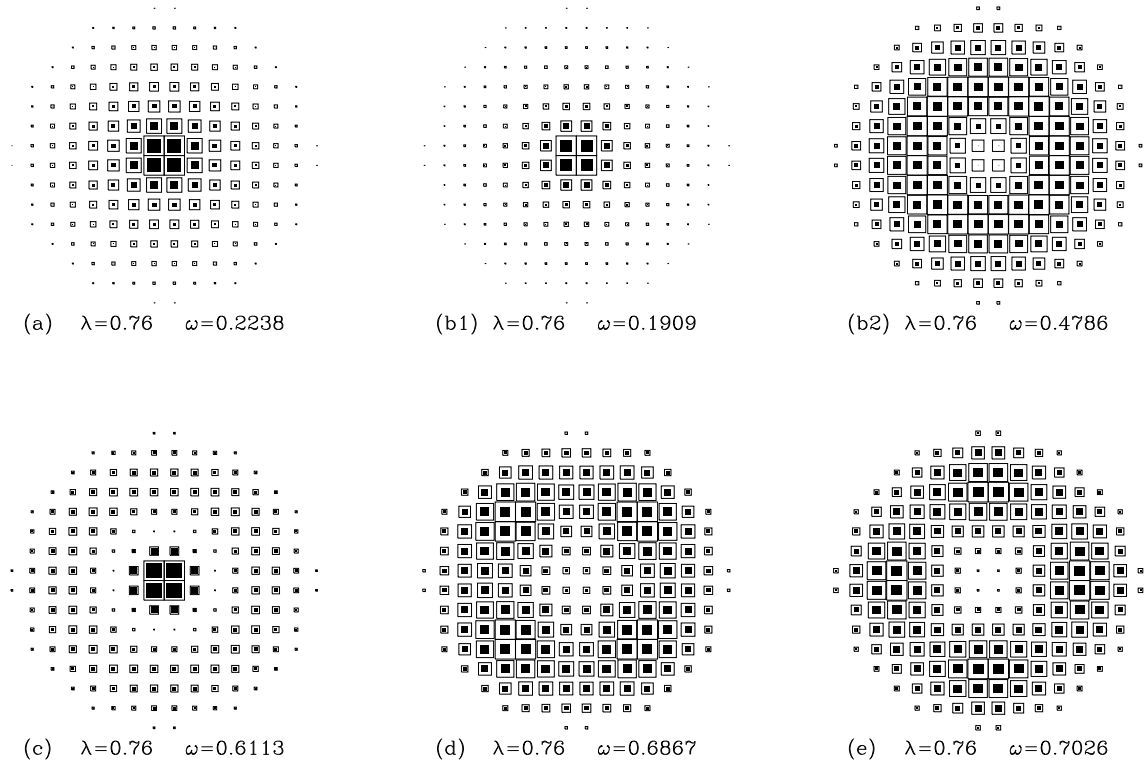


FIG. 9. Maps of the spin fluctuations in the square lattice system as in Fig. 7, but for $\lambda = 0.76$, above λ_c . The soft mode in (a) is strongly out-of-plane, with intensity concentrated near the vortex core, while mode (b)'s degeneracy is now split.

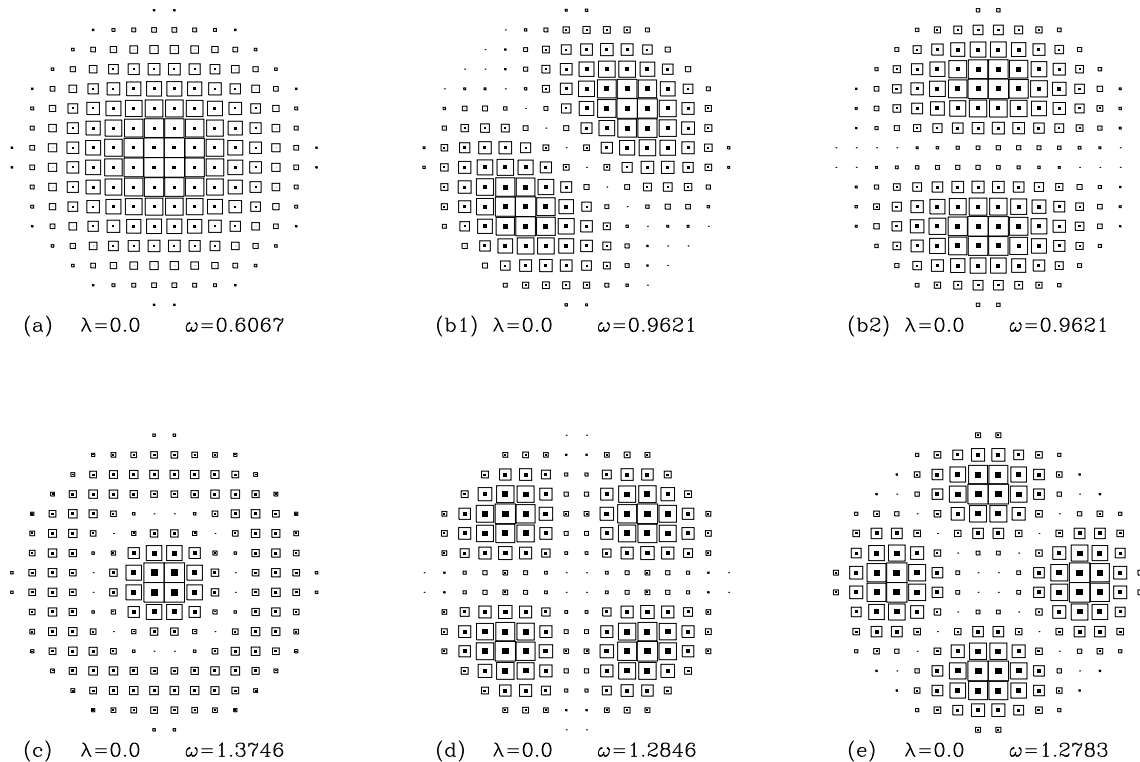


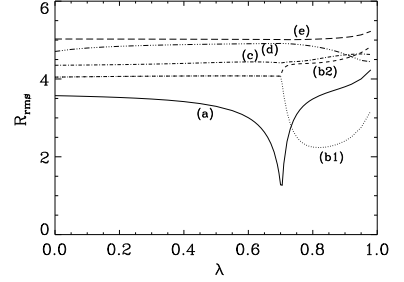
FIG. 10. Maps of the spin fluctuations in a square lattice system as in Fig. 7, but without a vortex present, for $\lambda = 0$. In comparing with Fig. 7, modes (b1), (b2), and (d) there have extra fluctuations present due to the vortex, at its core, not seen here in the absence of the vortex.

To study the tendency of the vortex to concentrate a mode near its core, we define the *rms* spread R_{rms} of a wavefunction using the total in-plane plus out-of-plane fluctuations as a weighting factor, as follows;

$$R_{\text{rms}}^2 = \frac{\sum_{\mathbf{n}} (|w_{k,\mathbf{n}}^1|^2 + |w_{k,\mathbf{n}}^2|^2) [(x_{\mathbf{n}} - x_0)^2 + (y_{\mathbf{n}} - y_0)^2]}{\sum_{\mathbf{n}} (|w_{k,\mathbf{n}}^1|^2 + |w_{k,\mathbf{n}}^2|^2)}. \quad (5.2)$$

In a similar way, the *rms* spread of the system itself can be evaluated by using a constant weighting factor. For the system with 180 sites that is discussed in Figs. 7, 8, and 9, the *rms* spread of the system is 5.355 lattice constants. The *rms* spreads of the lowest frequency wavefunctions are shown in Fig. 11. There is a substantial reduction in R_{rms} for the soft mode as $\lambda \rightarrow \lambda_c$, while for the other modes there tends to be less drastic changes. Only mode (b1), which crosses the soft mode (a) slightly above λ_c , shows a similar sized change. Because the soft mode has an *rms* spread much smaller than the *rms* spread of the system for λ near λ_c , we interpret this to mean that the soft mode is a mode localized on the vortex, while the other lowest modes are more extended over the whole system. It is possible that there could be other modes higher up in the spectrum which are also localized in this sense, but it could be difficult to detect them because of the limited size of the systems that can be easily solved numerically.

FIG. 11. The *rms* spreads of the 6 lowest frequency wavefunctions for the square lattice system with 180 sites, versus anisotropy parameter λ . The letters refer to the modes shown in Figs. 4–6. For the lattice itself, $R_{\text{rms}} = 5.355$, while the radius of the system is about 8 lattice constants.



VI. RESULTS: TRIANGULAR AND HEXAGONAL LATTICES

For comparison, we have also calculated the spectra for finite circular systems on triangular and hexagonal lattices. The same methods as described above for the square lattice were used, in which the primary physical difference is the coordination number $z = 6$ for the triangular lattice, and $z = 3$ for the hexagonal lattice. This leads to the different values of $\lambda_c \approx 0.62$ for the triangular lattice, and $\lambda_c \approx 0.84$ for the hexagonal lattice, as seen in the spectra shown in Fig. 12. These results are completely consistent with the Ansatz calculation for this mode.²³ There are substantial similarities in the spectra for the different lattices, including the splitting of the degeneracies for $\lambda > \lambda_c$, the modes with downward cusps at $\lambda = \lambda_c$, and the one component of the lowest degenerate pair coming close to zero frequency somewhat above λ_c . On the other hand, the symmetries of the lattices lead to small differences in the wavefunctions (not shown here).

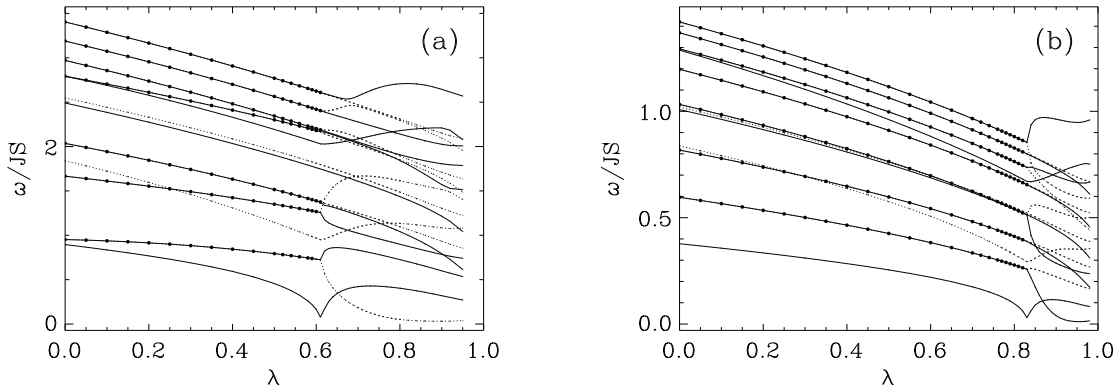


FIG. 12. Normal mode spectra (lowest 19 modes) of circular systems containing a vortex at the center, with fixed boundary conditions, for (a) triangular lattice with 174 sites; (b) hexagonal lattice with 192 sites. While many features of these results also appear in Fig. 2, the different values of λ_c are notable.

VII. DISCUSSION AND CONCLUSIONS

Through numerical diagonalization of the spin equations of motion linearized about a non-uniformly magnetized state, we have found the spinwave spectrum for finite circular systems containing a single vortex at the center. The spectrum shows some important dynamical properties of individual magnetic vortices. The most significant feature is the presence of a particular mode [mode (a) in the Figures] whose frequency comes close to zero near λ_c , and whose *rms* radius comes close to one lattice constant at the same time. For λ just below λ_c , such a localized mode has a time-dependent spin structure with radial dependence of its amplitude very similar to the *static* out-of-plane vortex structure present for λ just *above* λ_c . This is suggested by comparing the mode (a) in Fig. 8 and the lowest curve ($\lambda = 0.71$) in Fig. 1. Thus, this mode is the precursor to the instability of an in-plane vortex to become an out-of-plane vortex. This idea is further supported by the fact that the *rms* radius of mode (a) becomes comparable to the “vortex core” radius of an out-of-plane vortex for $\lambda = 0.70$, defined by,⁸

$$r_v = \frac{1}{2} \left(\frac{\lambda}{1-\lambda} \right)^{1/2}. \quad (7.1)$$

On the other hand, for λ far below λ_c , mode (a) bears a lot of similarity to the lowest mode when there is *no* vortex present. This can be seen by comparing Fig. 7a and Fig. 10a. However, in the absence of the vortex, this lowest mode undergoes no substantial changes as λ is increased, even through λ_c .

We have found that some of the higher modes also have strong changes associated with the vortex instability; partial evidence is the downward cusps in the spectrum.²⁷ Additional evidence appears in the wavefunctions themselves. For example, mode (c) (third lowest in Fig. 3b) is one of the modes with a cusp, and for $\lambda = 0$, there is not too much difference in this mode’s structure, regardless of the presence or absence of the vortex [compare Fig. 7c and Fig. 10c], except that the mode is more concentrated at the system center when the vortex is present. However, this mode also concentrates itself additionally onto the vortex core for λ near λ_c , just as mode (a) does, as seen in Fig. 8c. Presumably, the other modes higher up in the spectrum that possess downward cusps in their λ -dependences are also strongly affected by the vortex instability.

The crossover from in-plane to out-of-plane vortices exhibits itself in an even more obvious way. A significant fraction of the modes are degenerate for $\lambda < \lambda_c$, but *all* of these degeneracies split for $\lambda > \lambda_c$. These degeneracies must be associated with a symmetry of the in-plane vortex, that is broken in the out-of-plane vortex. For example, consider the lowest degenerate mode, (b), in Fig. 3b, for $\lambda < \lambda_c$. We might expect that a vortex in an infinite, continuum limit system would have a degenerate pair of zero-frequency modes associated with translation of its position in the two lattice directions. This pair would then be shifted to finite frequency on the discrete lattice, and when the vortex is additionally confined to a finite system as we have here, they would correspond to the two different directions along which the vortex center position could oscillate, rather than translate. But clearly, with this interpretation there is some problem to understand how this *spatial* symmetry could be broken in the out-of-plane vortex, or why the out-of-plane vortex wouldn’t have a degenerate pair of translation modes. On the other hand, it is known that the dynamical response of the out-of-plane vortex to an external force is substantially different from that for the in-plane vortex. This is because the the gyrovector (vorticity times S^z at vortex core) of the in-plane vortex is zero, but for the out-of-plane vortex it is nonzero¹⁵. However, one would still need to explain the additional symmetries associated with the other degeneracies as well.

A simpler way to view the degeneracies is that they are most closely associated with symmetries of the in-plane vortex in *spin* space, the most important of which is that it is invariant under reversal of the out-of-plane component, because that component is zero. Then, *all* of the degeneracies must somehow be associated with the symmetry of those modes under reversal of their out-of-plane spin components, $S^z \rightarrow -S^z$. For the in-plane vortex, this is equivalent to $S^{\tilde{y}} \rightarrow -S^{\tilde{y}}$. Once we have an out-of-plane vortex for $\lambda > \lambda_c$, the static vortex structure has all $S_{\mathbf{n}}^z$ either greater than 0 or all $S_{\mathbf{n}}^z$ less than 0. Then it is clear that the perturbations (specifically, $S^{\tilde{y}}$) about that static structure cost different energies depending on whether they increase or decrease each $S_{\mathbf{n}}^z$, leading to a breaking of the up-down S^z symmetry that was present in the in-plane vortex. However, thinking this way, there is still a problem to understand *which* of the modes would be in degenerate pairs for $\lambda < \lambda_c$.

To obtain one more way to understand the degeneracies, we can plot the complete wavefunctions, including the phase information. This can be done by drawing an arrow in the complex plane for each lattice site, where the length of the arrow is proportional to $|w_{k,\mathbf{n}}^1|$, and the direction of the arrow is determined by the phase of $w_{k,\mathbf{n}}^1$. Similar arrows can be drawn for the other component of the wavefunction, $w_{k,\mathbf{n}}^2$. For in-plane vortices, $w_{k,\mathbf{n}}^2$ represents the in-plane spin fluctuations, while $w_{k,\mathbf{n}}^1$ represents the out-of-plane spin fluctuations. For out-of-plane vortices, $w_{k,\mathbf{n}}^2$ represents only a part of the in-plane spin fluctuations, while $w_{k,\mathbf{n}}^1$ represents a combination of out-of-plane and in-plane spin fluctuations, depending on the static out-of-plane spin structure. This interesting representation of the two modes

(b1) and (b2) is shown in Fig. 13, for $\lambda = 0.40$, well below λ_c . Here we clearly see the distinction between these degenerate modes, which is made in terms of the phase of the spinwave and the way it changes around the center position of the vortex. Mode (b2) has the phase of *both* components $w_{k,\mathbf{n}}^1$ and $w_{k,\mathbf{n}}^2$ changing in the positive sense around the vortex center, while mode (b1) has the phase of both components changing in the negative sense around the vortex center. Of course, this representation is not unique; we could make linear combinations of these two modes and produce equivalent wavefunctions that do not have this “vortexlike” and “antivortex-like” appearance, but which would produce squared wavefunctions more like those already shown for $\lambda = 0$ in Fig. 7b1 and Fig. 7b2.

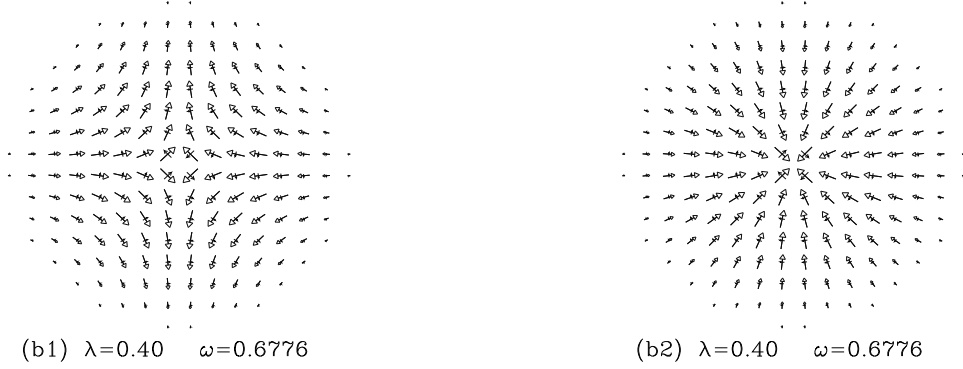


FIG. 13. Wavefunctions for the lowest degenerate modes (b1) and (b2) in the 180 site square lattice system with a vortex at the center, at $\lambda = 0.40$, well below λ_c . The line-head arrows are the complex amplitudes $w_{k,\mathbf{n}}^1$, and the hollow-head arrows are the complex amplitudes $w_{k,\mathbf{n}}^2$. The relative sizes and phases of these amplitudes are preserved in these diagrams. $w_{k,\mathbf{n}}^1$ relates to the out-of-plane spin fluctuations, and $w_{k,\mathbf{n}}^2$ relates to the in-plane spin fluctuations. The frequency of these modes is $\omega/JS=0.6776$.

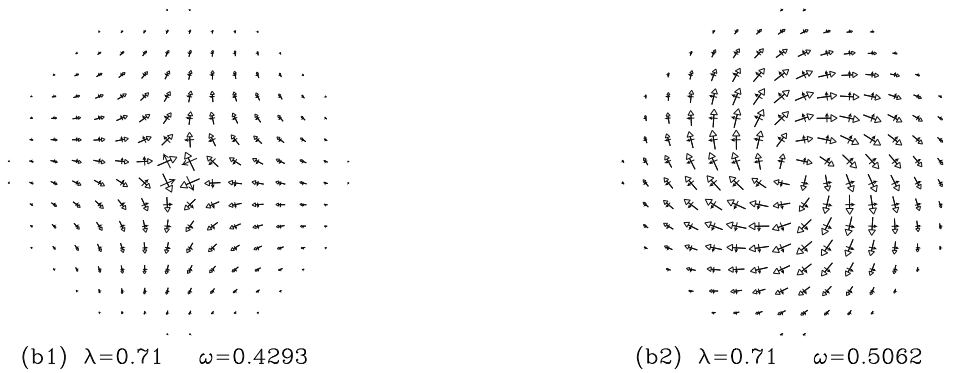


FIG. 14. Wavefunctions for the modes (b1) and (b2) in the 180 site system with a vortex at the center, as in Fig. 13, but for $\lambda = 0.71$, just above λ_c , where they are now nondegenerate. Mode (b1) has frequency $\omega_{b1}/JS = 0.4293$, and mode (b2) has frequency $\omega_{b2}/JS = 0.5062$.

This representation has the great advantage that it contains the physical explanation of how the symmetry is broken; for $\lambda > \lambda_c$, once there are static out-of-plane spin components, the two different senses of change in the spinwave phase are not equivalent. Then mode (b1), with its phase changing in the negative sense around the vortex center, falls lower than mode (b2). The two wavefunctions are shown in Fig. 14, for $\lambda = 0.71$, just above λ_c . Once there are nonzero S^z spin components in the static vortex structure, this lack of equivalence for the two senses of rotation of the phase is very reasonable. It can also explain the higher degenerate pairs, because they also have the spinwave phase changing smoothly as one moves around the vortex center, some with *higher winding numbers*—the phase change of the spinwave in these cases changes by $2\pi n$, where n is an integer [See Fig. 15]. Furthermore, this viewpoint shows why all of these degeneracies are split at λ_c , because the plus and minus senses of rotation of the phase are not equivalent, no matter what the winding number. Conversely, the modes that do not occur as degenerate pairs do not have a slow change in the phase around the vortex center. This new effect might be described as a coupling of the vorticity of the original vortex to the winding number of the phase of its spinwave excitations. Further details on the forms and characteristics of these wavefunctions will be published elsewhere.

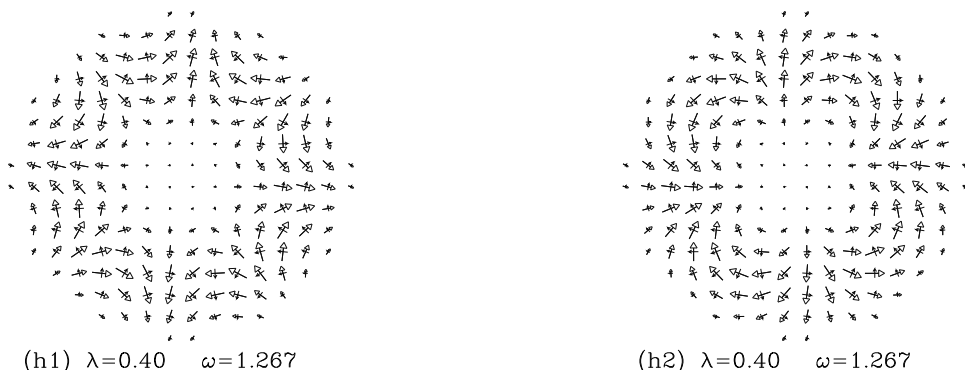


FIG. 15. Wavefunctions for the third lowest degenerate pair of modes of the 180 site system with a vortex at its center, as in Fig. 13, at $\lambda = 0.40$. The frequency of these modes is $\omega/JS = 1.267$, and they have winding numbers -3 and $+3$.

There are some finite size and boundary effects in these results that cannot be avoided, but that do not invalidate the results. For example, the choice of fixed boundary conditions eliminates the Goldstone mode related to global rotation of the spins in the XY plane that is present for free boundary conditions. However, the fixed boundary condition has the advantage that it reduces the spin fluctuations at the boundary, whereas the free boundary condition artificially enhances those boundary fluctuations. These are minor differences. The effect of the finite sized system, for the most part, can be understood to produce a finite frequency spacing between the modes, that becomes smaller as the reciprocal system length. This causes the frequency scale of the soft mode (a) at $\lambda = 0$, in Fig. 6, to go to zero for the infinite sized system, which is partly an artifact of the calculation, because this is the lowest mode for fixed boundary conditions. For the free boundary conditions, this soft mode lies higher up in the spectrum. In a real system of physical interest at some temperature above the Kosterlitz-Thouless temperature, we could not consider an isolated vortex and its normal modes, because entropic effects would always produce a length scale (i.e., correlation length) at which the nearest neighboring vortex would be found. Thus, it may not be necessary to consider the infinite sized system limit, because the neighboring vortices will produce an effective finite length scale over which we might think that the vortex is restricted.

In conclusion, we have found a rich structure in the spinwave modes of an individual vortex, and have shown how these modes are related to the instability of in-plane vortices to become out-of-plane vortices at λ_c . This information can be valuable for improving the description of the dynamics of interacting vortices in terms of their positions, and, the internal vibrational motions we have found. Because this is a zero-temperature single-vortex calculation, we can only speculate that it might be possible for the vortex instability to affect dynamical correlation functions. If there is an effect, it would be most prominent in the correlation function $S^{zz}(q, \omega)$ of the out-of-plane spin components, especially for a material whose anisotropy constant λ is near λ_c . It will be a future challenge to consider whether the

frequency spectra we have found can be related to these dynamic correlations in thermal equilibrium in a quantitative way.

VIII. ACKNOWLEDGMENTS

Discussions with Alan R. Bishop and F. G. Mertens are gratefully acknowledged. This work was supported in part by NSF grant DMR-9412300.

-
- ¹ See, for example, L.P. Regnault and J. Rossat-Mignod, *J. Magn. Magn. Mater.* **14**, 194 (1974); L.P. Regnault et al., *Physica B+C*, **136B**, 329 (1986); L.M. Falicov and J.L. Moran-Lopez, editors., "Magnetic Properties of Low-Dimensional Systems," Springer-Verlag, Berlin (1986).
- ² V.L. Berezinskii, *Sov. Phys. JETP* **34**, 610 (1972).
- ³ J.M. Kosterlitz and D.J. Thouless, *J. Phys. C* **6**, 1181 (1973); *ibid.*, *C* **7**, 1046 (1974).
- ⁴ D.L. Huber, *Phys. Lett.* **76A**, 406 (1980); *Phys. Rev. B* **26**, 3758 (1982).
- ⁵ F.G. Mertens, A.R. Bishop, G.M. Wysin and C. Kawabata, *Phys. Rev. Lett.* **59**, 117 (1987); *Phys. Rev. B* **39**, 591 (1989).
- ⁶ B.A. Ivanov and D.D. Sheka, *Phys. Rev. Lett.* **72**, 404 (1994).
- ⁷ S. Hikami and T. Tsuneto, *Prog. Theor. Phys.* **63**, 387 (1980).
- ⁸ M.E. Gouvêa, G.M. Wysin, A.R. Bishop and F.G. Mertens, *Phys. Rev.* **B39**, 11840 (1989).
- ⁹ A.R. Völkel, F.G. Mertens, A.R. Bishop and G.M. Wysin, *Phys. Rev.* **B43**, 5992 (1991).
- ¹⁰ F.G. Mertens, G. Wysin, A.R. Völkel, A.R. Bishop and H.J. Schnitzer, in "Nonlinear Coherent Structures in Physics and Biology," F.G. Mertens and K.H. Spatschek, eds., Plenum, New York (1994).
- ¹¹ A.R. Völkel, G.M. Wysin, F.G. Mertens, A.R. Bishop and H.J. Schnitzer, *Phys. Rev. B* **50**, 12,711, (1994).
- ¹² A.A. Thiele, *Phys. Rev. Lett.* **30**, 230 (1973); *J. Appl. Phys.* **45**, 377 (1974).
- ¹³ N. Papanicolaou and T.N. Tomaras, *Nucl. Phys. B* **360**, 425 (1991).
- ¹⁴ B.A. Ivanov and V.A. Stephanovich, *Phys. Lett. A* **141**, 89 (1989).
- ¹⁵ G.M. Wysin and F.G. Mertens, in *Nonlinear Coherent Structures in Physics and Biology*, Lecture Notes in Physics **393**, Springer-Verlag, Berlin (1991); G.M. Wysin, F.G. Mertens, A.R. Völkel and A.R. Bishop, in *Nonlinear Coherent Structures in Physics and Biology*, Plenum, New York (1994).
- ¹⁶ A.M. Kosevich, *Sov. Phys. Usp.* **7**, 837 (1965).
- ¹⁷ J.R. Currie, J.A. Krumhansl, A.R. Bishop and S.E. Trullinger, *Phys. Rev.* **B22**, 477 (1980).
- ¹⁸ R. Boesch, P. Stanicoff and C.R. Willis, *Phys. Rev. B* **38**, 6713 (1988); R. Boesch and C.R. Willis, *Phys. Rev. B* **42**, 6371 (1990).
- ¹⁹ G.M. Wysin, M.E. Gouvêa, A.R. Bishop and F.G. Mertens, in "Computer Simulations Studies in Condensed Matter Physics," D.P. Landau et al., eds., Springer-Verlag, Berlin (1988).
- ²⁰ B.V. Costa, M.E. Gouvêa and A.S.T. Pires, *Phys. Lett. A* **165**, 179 (1992).
- ²¹ A.R. Pereira, A.S.T. Pires and M.E. Gouvêa, *Solid St. Comm.* **86**, 187 (1993).
- ²² A.R. Pereira, A.S.T. Pires and M.E. Gouvêa, *J. Magn. Magn. Mater.* **134**, 121 (1994).
- ²³ G.M. Wysin, *Phys. Rev. B* **49**, 8780 (1994).
- ²⁴ A.R. Völkel, unpublished results (1991).
- ²⁵ I.U. Heilmann, J.K. Kjems, Y. Endoh, G.F. Reiter and G. Shirane, *Phys. Rev. B* **24**, 3939 (1981).
- ²⁶ T.Holstein and H. Primakoff, *Phys. Rev. B* **58**, 1098 (1940).
- ²⁷ In contrast to modes (a) which becomes soft at $\lambda = \lambda_c$, the cusps at λ_c for the higher modes remain at finite frequencies.

FIG. 1. Profiles of S^z vs. distance r from the vortex center, for single static out-of-plane vortices at the center of a circular system with 180 sites on a square lattice. The curves are labelled by the different values of λ . These results were obtained by the relaxation procedure described in the text (Sec. II), using a fixed boundary condition as described in Sec. IV.

FIG. 2. Diagram showing the relation between the original xyz -coordinate system, and the local coordinates, $\tilde{x}\tilde{y}\tilde{z}$, where the \tilde{z} -axis lies along the direction of the spin at a particular site in the unperturbed vortex, and the \tilde{x} -axis lies in the xy -plane.

FIG. 3. Comparison of the lowest 19 modes in the spinwave spectrum for a square lattice circular system with 180 sites, containing an in-plane vortex at its center, with (a) free boundary conditions, and (b) fixed boundary conditions. Degenerate modes are marked with solid circles. The solid and dotted lines are used only to distinguish nearby modes.

FIG. 4. Comparison of the lowest 19 modes in the spinwave spectrum for a square lattice circular system with 492 sites, with fixed boundary conditions, (a) containing an in-plane vortex at its center, and (b) no vortex (spinwave modes about ferromagnetically aligned state). The solid and dotted lines are used only to distinguish nearby modes.

FIG. 5. Asymptotic least square fits (solid curves) of the frequency of the soft mode (data points) for square lattice circular systems with 12, 68, and 492 spins, using the functional form $\omega = \hat{\omega}(1 - \lambda/\lambda_c)^{1/2}$. Only the data with λ very close to λ_c were used to obtain the fitted curves. This functional form fits well over the full range of λ only for small systems ($N \leq 24$).

FIG. 6. Size dependence of the soft mode for square lattice circular systems with N sites, using fixed boundary conditions. The frequency ω_o of the soft mode at $\lambda = 0$ is shown on a log-log plot, and compared with an asymptotic fit to the function, $\omega_o = 6.92N^{-0.475}$. This is close to a linear dependence on inverse system diameter.

FIG. 7. Maps of the spin fluctuations in a square lattice system with 180 sites, for the six lowest frequency modes when $\lambda = 0.0$. Out-of-plane fluctuations $\langle (\delta S_{\mathbf{n}}^{\text{out}})^2 \rangle$ (Eq. 3.13b) are proportional to the areas of the solid squares. In-plane fluctuations $\langle (\delta S_{\mathbf{n}}^{\text{in}})^2 \rangle$ (Eq. 3.13a) are proportional to the white area within the larger squares. The total in-plane plus out-of-plane fluctuations are proportional to the areas of the larger squares. Part (a) shows the soft mode, while (b1) and (b2) are a degenerate pair, and (c), (d) and (e) are the next higher frequency modes.

FIG. 8. Maps of the spin fluctuations in the square lattice system as in Fig. 7, but for $\lambda = 0.69$, just below the transition to an out-of-plane vortex. In (a), the soft mode's intensity concentrates itself more near the vortex core, and is strongly out-of-plane, while the higher modes in (b) through (e) have much smaller changes from their $\lambda = 0.0$ forms.

FIG. 9. Maps of the spin fluctuations in the square lattice system as in Fig. 7, but for $\lambda = 0.76$, above λ_c . The soft mode in (a) is strongly out-of-plane, with intensity concentrated near the vortex core, while mode (b)'s degeneracy is now split.

FIG. 10. Maps of the spin fluctuations in a square lattice system as in Fig. 7, but without a vortex present. In comparing with Fig. 7, modes (b1), (b2), and (d) there have extra fluctuations present due to the vortex, at its core, not seen in the absence of the vortex.

FIG. 11. The rms spreads of the 6 lowest frequency wavefunctions for the square lattice system with 180 sites, versus anisotropy parameter λ . The letters refer to the modes shown in Figs. 4–6. For the lattice itself, $R_{\text{rms}} = 5.355$, while the radius of the system is about 8 lattice constants.

FIG. 12. Normal mode spectra (lowest 19 modes) of circular systems containing a vortex at the center, with fixed boundary conditions, for (a) triangular lattice with 174 sites; (b) hexagonal lattice with 192 sites. While many features of these results also appear in Fig. 2, the different values of λ_c are notable.